



Spherule layers, crater scaling laws, and the population of ancient terrestrial impactors



Brandon C. Johnson^{a,1,*}, Gareth S. Collins^b, David A. Minton^c, Timothy J. Bowling^c,
Bruce M. Simonson^d, Maria T. Zuber^a

^a Department of Earth, Atmospheric and Planetary Sciences, Massachusetts Institute of Technology, 77 Massachusetts Avenue, Cambridge, MA 02139, USA

^b Impacts and Astromaterials Research Centre, Dept. Earth Science and Engineering, Imperial College London, London SW7 2AZ, UK

^c Department of Earth, Atmospheric, and Planetary Sciences, Purdue University, 550 Stadium Mall Drive, West Lafayette, IN 47907, USA

^d Geology Department, Oberlin College, Oberlin, Ohio 44074, USA

ARTICLE INFO

Article history:

Received 2 June 2015

Revised 8 February 2016

Accepted 9 February 2016

Available online 19 February 2016

Keywords:

Cratering

Earth

Moon

Near-Earth objects

Planetary dynamics

ABSTRACT

Ancient layers of impact spherules provide a record of Earth's early bombardment history. Here, we compare different bombardment histories to the spherule layer record and show that 3.2–3.5 Ga the flux of large impactors (10–100 km in diameter) was likely 20–40 times higher than today. The E-belt model of early Solar System dynamics suggests that an increased impactor flux during the Archean is the result of the destabilization of an inward extension of the main asteroid belt (Bottke et al., 2012). Here, we find that the nominal flux predicted by the E-belt model is 7–19 times too low to explain the spherule layer record. Moreover, rather than making most lunar basins younger than 4.1 Gyr old, the nominal E-belt model, coupled with a corrected crater diameter scaling law, only produces two lunar basins larger than 300 km in diameter. We also show that the spherule layer record when coupled with the lunar cratering record and careful consideration of crater scaling laws can constrain the size distribution of ancient terrestrial impactors. The preferred population is main-belt-like up to ~50 km in diameter transitioning to a steep distribution going to larger sizes.

© 2016 Elsevier Inc. All rights reserved.

1. Introduction

The constant recycling of Earth's crust by plate tectonics makes it impossible to use observations of terrestrial craters to determine if and how the impactor flux changed throughout Earth's history (Johnson and Bowling, 2014). Fortunately, very large impacts create distal ejecta layers with global extent (Smit, 1999). Even when the source crater has been destroyed, these layers can act as a record of the impacts that created them (Simonson and Glass, 2004). Although some impact ejecta layers are more proximal material transported as part of the ballistic ejecta curtain, many of the layers are distal deposits produced by impact (vapor) plumes (Glass and Simonson, 2012; Johnson and Melosh, 2014; 2012a; Simonson and Glass, 2004). Estimates of the size of the impactors that created these impact plume layers suggest that the impactor

flux was significantly higher 2.4–3.5 Ga than it is today, although these flux estimates are mostly qualitative (Johnson and Melosh, 2012b).

The Early Archean to earliest Paleoproterozoic spherule layers formed well after the Late Heavy Bombardment (LHB) (because almost all the layers are Early or Late Archean in age, we refer to them collectively as Archean from here on for the sake of convenience). The LHB is thought to have ended after the formation of the lunar basin Orientale, about 3.7 Ga (Stöffler and Ryder, 2001). The Nice model is a dynamical model of the evolution of the orbits of the outer giant planets that has been used to explain the LHB through a destabilization of the main asteroid belt by abrupt migration of the giant planets (Gomes et al., 2005). The E-belt model, which includes an inward extension of the main asteroid belt from about 1.7–2.1 AU, was developed to explain the formation of the Archean spherule layers (Bottke et al., 2012).

Bottke et al. (2012) compare the expected number of Chicxulub-sized craters on Earth over the timespans where spherule-bearing sedimentary sequences have been found in the Archean. The E-belt model assumes 6 km diameter bodies striking at 22 km/s create “Chicxulub sized” (~160-km diameter) craters on Earth (Bottke et al., 2015). According to Johnson and Melosh (2012b),

* Correspondence to: Department of Earth, Environmental and Planetary Sciences, Brown University, 324 Brook Street, Box 1846, Providence, RI 02912, USA. Tel.: +1 401 863 5163.

E-mail address: Brandon_Johnson@Brown.edu (B.C. Johnson).

¹ Department of Earth, Environmental and Planetary Sciences, Brown University, 324 Brook Street, Providence, RI 02912, USA

a 6-km diameter impactor would make a sparse spherule layer only 0.09–0.2-mm thick. However, the observed Archean spherule layers are centimeters to 10's of centimeters thick and were likely created by impactors that are ~10–90 km in diameter (Johnson and Melosh, 2012b; Kyte et al., 2003; Lowe et al., 2003, 2014; Lowe and Byerly, 2015). In Section 2, using the method of Johnson and Melosh (2012b), we estimate the sizes of the impactors that created each of the Archean spherule layers. We then compare this record to different possible bombardment histories. We find that the nominal flux predicted by the E-belt model is 7–19 times too low to produce the Archean spherule layers.

In Section 3 we show that careful application of crater scaling laws provides a reasonably consistent relationship (<10% discrepancy) between crater size and impactor properties that is in excellent agreement with recent numerical models of terrestrial crater formation. Then, as an additional test of the E-belt model, we calculate the impactor size required to produce a 160-km diameter “Chicxulub sized” crater on Earth. Contrary to the 6 km diameter impactor estimate of Bottke et al. (2012), a ~13 km diameter impactor is required to produce a 160-km diameter crater on Earth at an impact speed of ~22 km/s. The approximately factor of two discrepancy in impactor size implies that the Bottke et al. (2012) E-belt flux is overestimated by a factor of 7.5–10. In this scenario, the nominal E-belt model produces only two craters larger than 300 km in diameter on the Moon rather than most of the LHB basins (Bottke et al., 2012; Morbidelli et al., 2012).

Finally in Section 4 we combine constraints on the impactor Size Frequency Distribution (SFD) with constraints from the lunar cratering record. We find that the population of ancient impactors that is roughly main-belt like from ~1–30 km in diameter but steeper than the main-belt SFD at larger sizes is consistent with the lunar cratering record and the terrestrial impact record from spherule layers.

2. Spherule layer constraints on terrestrial bombardment

Observations of NEOs provide a direct estimate of the present-day impactor flux (Stuart and Binzel, 2004, Fig. 1). For objects greater than 10 km in diameter, these estimates suffer from small number statistics. Because asteroids larger than ~10 km in diameter are delivered to the NEO population predominantly by the size-independent effect of dynamical chaos, we expect little difference between NEO and main-belt size distributions for objects larger than 10 km in diameter (Minton and Malhotra, 2010). Thus, we scale the main-belt SFD (Minton, Richardson and Fassett, 2015b) to be equal to the NEO SFD for a 10-km diameter object (Fig. 1). We then assume the actual current impactor flux is the maximum of these two curves, which is a similar method to that used by Le Feuvre and Wieczorek (2011). This combined impactor SFD allows us to compare different bombardment histories to the spherule layer record, which predicts some impactors were substantially larger than 30 km in diameter. We note that the size above which we expect the impactor SFD to appear main-belt like is not strictly constrained. Additionally, there is only a small size range where both distributions are well determined (i.e. the main belt population is poorly constrained for bodies smaller than a few km in diameter while above a few km in size the NEO population suffers from poor statistics). However, the errors associated with flux estimates based on the spherule layer record are likely much larger than any uncertainty associated with our estimates of the current day impactor SFD.

Fig. 2 shows the cumulative number of impacts by bodies larger than 10 km in diameter for three bombardment histories. The decreasing flux estimate is based on dynamical erosion of the asteroid belt (Minton and Malhotra, 2010) and is scaled so that the current impactor flux is equal to the impactor flux calculated

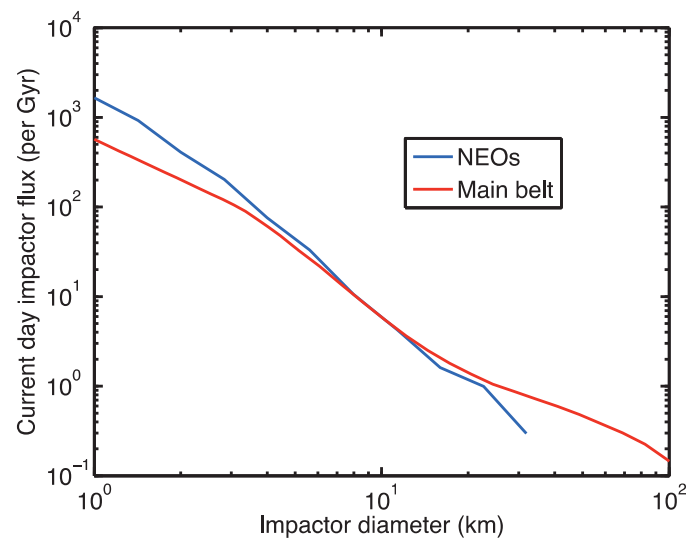


Fig. 1. The cumulative rate of impacts larger than a given size as a function of impactor diameter. The blue curve is the current impactor flux based on observations of NEOs (Stuart and Binzel, 2004). We note that the impactor flux estimates of Stuart and Binzel (2004) are in excellent agreement with more recent estimates in this size range (Harris and D’Abramo, 2015). The red curve is the main belt asteroid belt size frequency distribution (Minton et al., 2015b) scaled so that it is equal to the impactor flux of NEOs for bodies with 10 km diameter. (For interpretation of the references to color in this figure legend, the reader is referred to the web version of this article.)

based on observations of NEOs (Stuart and Binzel, 2004). One minor difference between this work and that of Minton and Malhotra (2010) is that we have shifted the starting time of the decay of the main asteroid belt from 4.0 Ga to 4.5 Ga. Because we normalize the flux rate so that the current flux is equal to the estimates based on NEO observations, this change only reduces the flux estimates by a factor of less than two during the times of interest. The impact velocity of 22 km/s for E-belt impactors (Bottke et al., 2015; 2012) is not significantly different from 20.3 km/s, the mean impact velocity of asteroids impacting the Earth (Minton and Malhotra, 2010). According to Eq. (1), this difference in impact velocity only changes the transient crater size by 3.6%. Thus, we can safely ignore the slightly higher velocity of E-belt impactors and directly compare the number of impacting bodies of a given size when comparing different flux estimates.

The nominal E-belt model assumes that destabilization of the E-belt occurs 4.1 Ga, however, this timing is not strictly constrained (Bottke et al., 2012; Morbidelli et al., 2012). In the context of the Nice model, a destabilization of the E-belt 3.9 Ga corresponds to the lunar cataclysm view of the LHB, where almost all lunar basins formed about 3.9 Ga (Morbidelli et al., 2012). Moving the destabilization any later than that would imply that the Nice model cannot explain the LHB. Thus, we include flux estimates for destabilization at 4.1 Ga and 3.9 Ga to encompass the entire range of possible destabilization times (Fig. 2).

As Table 1 shows, the age of the ancient spherule layers cluster between 2.49–2.63 Ga and 3.23–3.47 Ga. To compare the flux to the number of spherule layers, we assume that the clustering is purely the result of strata from these two periods being well searched and particularly suited to preserving spherule layers. The average time between large impacts is about 0.05 Gyr between 2.49–2.63 Ga and about 0.03 Gyr between 3.23–3.47 Ga. To account in some crude way for the fact that impacts are Poisson distributed we add the average recurrence rate to both sides of the respective period. More precisely we assume the spherule layer record is complete between 2.44–2.68 Ga and 3.2–3.5 Ga. This means that there may be several undiscovered, destroyed, or

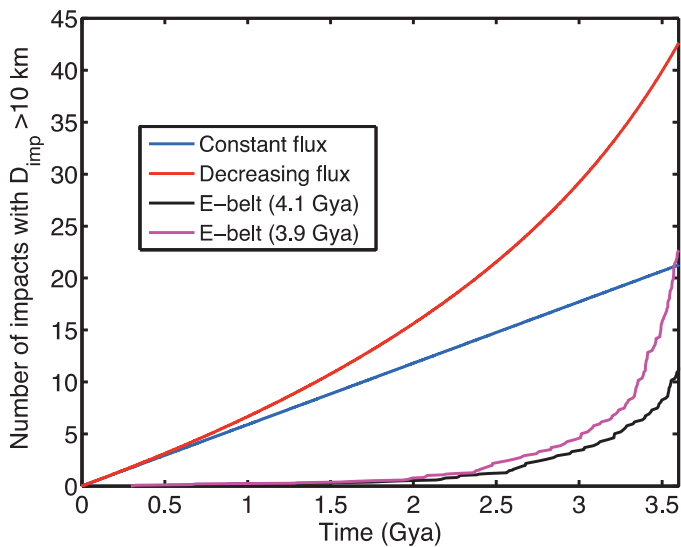


Fig. 2. Cumulative number of impactors larger than 10 km in diameter that hit the Earth. The blue line is calculated assuming a constant impactor flux equal to the current impactor flux (Stuart and Binzel, 2004). The red curve assumes the constantly decreasing impactor flux estimated by Minton and Malhotra (2010). The flux rate from Minton and Malhotra (2010) is normalized so that the current flux is equal to the estimates based on NEO observations (Stuart and Binzel, 2004). The purple and black curves are the cumulative number of “E-belt” impactors assuming a destabilization at 3.9 Ga and 4.1 Ga, respectively (Bottke et al., 2012). Note that the E-Belt impact curves were generated using a very simple model for the migration of the giant planets, and therefore the decay curves could potentially be different if a more realistic evolution of the outer planets were considered. Note that including impacts out to 3.9 Ga, the cumulative bombardment from the nominal E-belt model (purple) exceeds the value implied by a decreasing main belt flux (red) by a factor of 2.6. (For interpretation of the references to color in this figure legend, the reader is referred to the web version of this article.)

Table 1

Archean spherule layers. The layer thickness and age estimates for S5–S8 come from (Lowe et al., 2014) while all others are from Glass and Simonson (2012). The layers with multiple names are layers found at multiple localities that were likely created by the same impact (Glass and Simonson, 2012). For these “multiple” layers we report the entire range of layer thicknesses. The aggregate thickness is an estimate of how thick a layer composed of closely packed spherules would be. Aggregate thickness is the same as reduced layer thickness used in (Johnson and Melosh, 2012b). The impactor diameter is then calculated based on layer thickness using the same method as Johnson and Melosh (2012b).

Name	Approximate age (Ga)	Aggregate thickness (cm)	Impactor Diameter (km)
Dales Gorge & Kuruman	2.49	0.5–6	11–39
Bee Gorge	2.54	1–3	13–31
Reivilo & Paraburdoo	2.54–2.56	2–2.5	17–29
Jeerinah, Carawine, & Monteville	2.63	0.4–30	10–67
S5	3.23	20–50	37–79
S4	3.24	12	31–49
S3	3.24	30	42–67
S2	3.26	10–70	29–88
S6	3.26–3.30	20–50	37–79
S8	3.30	20–50	37–79
S7	3.42	20–50	37–79
S1 & Warrawoona	3.47	5–6	23–39

obscured layers that formed between 2.68 and 3.2 Ga, but that we have found all of the layers that formed between 2.44–2.68 Ga and 3.2–3.5 Ga. We note this assumption may produce a conservative estimate of impactor flux because there may be more layers within the strata that have already been searched. For example, Mohr-Westheide et al. (2015) and Koeberl, Schulz and Reimold (2015a,b) report on newly discovered Early Archean spherule layers in South

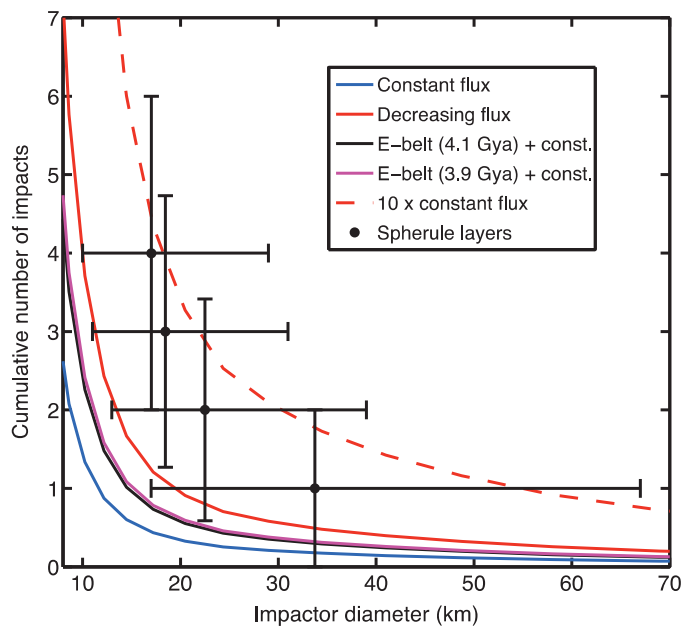


Fig. 3. Cumulative number of impacts larger than a given size plotted as a function of impactor diameter. The curves all represent the number of impacts between 2.44–2.68 Ga predicted by different dynamical models as indicated by the legend. The black and purple curves are the cumulative number of impacts from the E-belt added to the number expected from the constant flux scenario. The points with error bars represent the range of SFDs allowed by the spherule layer data from Table 1. The horizontal error bars connect the two SFDs assuming the minimum and maximum size estimates in Table 1. The vertical error bars assume Poisson statistics ($1-\sigma$ error of \sqrt{N} where N is the number of layers). Although these errors should technically be on the flux estimates they provide a sense of the ranges of impactor flux that could explain the abundance of spherule layers. (For interpretation of the references to color in this figure legend, the reader is referred to the web version of this article.)

Africa that may be distinct from any of those previously reported by Lowe et al. (2003, 2014).

By convolving the cumulative number of impacts from Fig. 2 with the assumed probability of layer preservation and discovery, we can estimate the number of spherule layers that a given bombardment history predicts. Note, the spherule layer record does not rule out a scenario where the impactor flux was high 2.44–2.68 Ga, low from 2.68–3.2 Ga, and high from 3.2–3.5 Ga. However, such a bombardment history is inconsistent with any of the dynamical models we consider (Bottke et al., 2012; Minton and Malhotra, 2010) and the terrestrial cratering record provides no evidence of periodic increases in impactor flux (Bailer-Jones, 2011). On shorter time scales, however, asteroid disruption events can produce increases in the flux of terrestrial impactors, as demonstrated by the formation of the Flora asteroid family, which has been linked to an increased impactor flux in the Ordovician (Nesvorný et al., 2007). It is unclear whether even larger disruption events could deliver enough material to explain the formation of the Archean spherule layers.

In Fig. 3, we compare the flux implied by the four layers that formed 2.44–2.68 Ga to the various bombardment histories shown in Fig. 2. Assuming the spherule layers are made by the smallest impactor sizes given in Table 1 and including the entire range of random variation implied by Poisson statistics (vertical error bars \sqrt{N}), the spherule layers are consistent with all the bombardment histories in Fig. 2 including a constant flux scenario. At the large end of the size range in Table 1, the spherule layers imply a flux from 2.44–2.68 Ga that is more than 10 times higher than the current impactor flux. At the low end of the size estimates from Table 1, however, the flux from 2.44–2.68 Ga is consistent with even the current day flux.

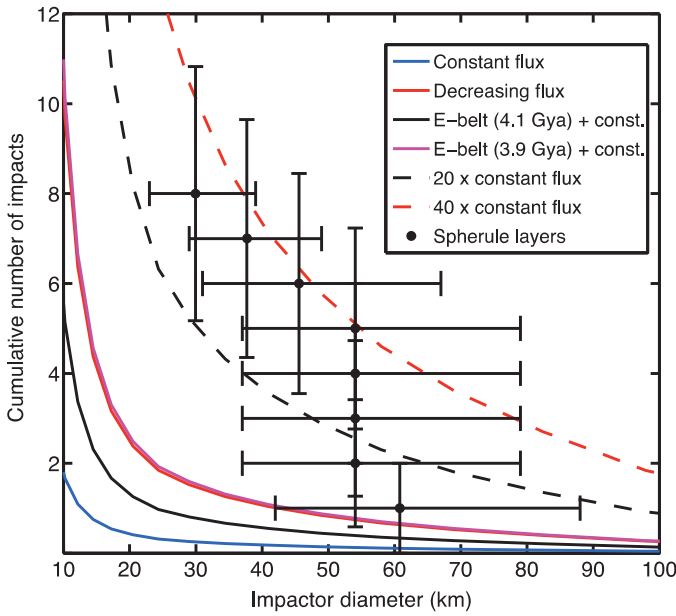


Fig. 4. Cumulative number of impacts larger than a given size plotted as a function of impactor diameter. The curves all represent the number of impacts between 3.2–3.5 Ga predicted by different dynamical models as indicated by the legend. The black and purple curves are the cumulative number of impacts from the E-belt added to the number expected from the constant flux scenario. The points with error bars represent the range of SFDs allowed by the spherule layer data from Table 1. The horizontal error bars connect the two SFDs assuming the minimum and maximum size estimates in Table 1. The vertical error bars assume Poisson statistics ($1\text{-}\sigma$ error of \sqrt{N} where N is the number of layers). Although these errors should technically be on the flux estimates they provide a sense of the ranges of impactor flux that could explain the abundance of spherule layers. (For interpretation of the references to color in this figure legend, the reader is referred to the web version of this article.)

In Fig. 4, we compare the flux implied by the eight layers that formed 3.2–3.5 Ga to the various bombardment histories shown in Fig. 2. We find the spherule layers are consistent with a flux significantly higher than any bombardment history in Fig. 4. Assuming the destabilization of the E-belt occurred at 4.1 Ga the E-belt flux during the time of spherule layer formation is 2.1 times the current impactor flux. Note that E-belt flux refers to the flux of impactors from the extension of the asteroid belt alone as shown in Fig. 2. Assuming the E-belt model is correct, the E-belt flux is in addition to some background flux of material coming from the main belt. In Figs. 3 and 4, we plot the sum of the E-belt flux and the constant flux model. In the text however, we also consider adding the E-belt flux to the decreasing flux of Minton and Malhotra (2010). If we instead assume the E-belt destabilized 3.9 Ga, the E-belt flux is 5.1 times higher than the current impactor flux during the period of spherule layer formation. The average flux from the decreasing flux model is 5.8 times the constant flux model. We find that a total impactor flux that is $\sim 20\text{--}40$ times the current, constant, impactor flux is required to explain the Archean Spherule layers (dashed lines; Fig. 4). We note the SFD inferred from the spherule layers looks different from that of the main belt; we will return to this in Section 4.

Assuming the flux from the main belt is given by the constant flux model, the E-belt flux would need to be 19–39 times the current impactor flux from 3.2–3.5 Ga to produce the spherule layers that formed during this period. This corresponds to 9.0–19 times the E-belt flux assuming destabilization occurred 4.1 Ga and 3.7–7.6 times if destabilization occurred 3.9 Ga. If instead we assume the flux from the main belt is given by the decreasing flux of Minton and Malhotra (2010), the E-belt flux would need to be 14–34 times the current current impactor flux from 3.2–3.5 Ga to

produce the spherule layers that formed during this period. This corresponds to 6.7–16 times the E-belt flux assuming destabilization occurred 4.1 Ga and 2.7–6.7 times if destabilization occurred 3.9 Ga. The Hungaria asteroids are thought to be the only survivors of the E-belt (Bottke et al., 2012). Because the current population of Hungarias is so small, statistics allow an E-belt flux that was a factor of two higher than the nominal case (Bottke et al., 2012). Even with a doubling in flux, the E-belt flux is too low to explain the formation of the Archean spherule layers.

3. Crater scaling laws

A principal constraint used to test any impact flux model is the observed number of impact basins on Earth and the Moon. For example, Bottke et al. (2012) used the observed number of post-LHB “Chicxulub-scale” ($D > 160$ km) impact craters on Earth and the Moon as a test of their E-belt impact flux model. Crucially, to convert a theoretical impactor SFD into a crater SFD requires a recipe for predicting the size of the final crater formed by the collision of an impactor of known mass, velocity and angle onto a planetary surface of known density and gravity. While this procedure is straightforward for small, simple bowl-shaped craters, it is complicated greatly by the process of crater modification (collapse) that becomes increasingly prevalent as crater size increases and internal crater morphology departs more and more from a simple bowl. As a result, several frameworks have been described and used in the literature, based on different observational constraints and assumptions about the nature of crater collapse, to predict the amount of enlargement that occurs during crater modification. While misapplication of these different approaches provides scope for disparate results, here we show that their careful application provides a reasonably consistent relationship ($<10\%$ discrepancy) between crater size and impactor properties that is in excellent agreement with recent numerical models of terrestrial crater formation. In Section 5, we apply this framework to compare the flux inferred from spherule layers to the lunar cratering record.

Estimating crater size from impactor and target properties is conventionally done in two steps. First, equations derived using the point-source approximation and dimensional analysis relate impactor and target properties to the diameter of the so-called transient crater (Holsapple, 1993; Holsapple and Schmidt, 1982). These equations are constrained by laboratory-scale impact experiments (Schmidt and Housen, 1987) and numerical models. As its name indicates, the transient crater is the short-lived bowl-shaped cavity excavated during the early stages of impact, which is modified by gravity-driven collapse of the transient crater walls and floor.

The diameter of the transient crater, D_{trans} , measured at the pre-impact target surface, is given by the following equation from Collins et al. (2005) and references therein:

$$D_{trans} = 1.161 \left(\frac{\rho_{imp}}{\rho_{targ}} \right)^{\frac{1}{3}} D_{imp}^{0.78} v_{imp}^{0.44} g^{-0.22} \sin^{\frac{1}{3}}(\theta), \quad (1)$$

where ρ_{imp} is impactor density, ρ_{targ} is target density, D_{imp} is impactor diameter, v_{imp} is impact velocity, g acceleration due to gravity, and θ is the impact angle measure with respect to the target surface (90° for a vertical impact and 0° for a grazing impact). All of the quantities in Eq. (1) are in MKS units. This equation is valid for gravity-scaled craters, meaning the weight of the excavated material is the principal force arresting crater growth. On Earth, Eq. (1) is valid for impactors larger than about one meter in diameter (Holsapple, 1993). This equation also assumes the impact is into a target with no appreciable porosity. We note again that the impactor size, velocity and gravity dependencies (exponents) in this equation are constrained by laboratory-scale impact experiments (e.g., Schmidt and Housen, 1987).

Table 2
Complex crater enlargement model parameters.

Model	η	A	γ
Croft (1985)	0.123–0.234	1	1
Croft (1985); modified	0.123–0.234	1.28–1.32	1.25
Schenk and McKinnon (1985) ¹	0.13	1.17	1.15
“ modified	0.13	1.29	1.25
Holsapple (1993)	0.086	1.35	1.32

Bold values are specified; remaining parameter is implied.

¹ Description of the Schenk and McKinnon (1985) model is also presented in McKinnon and Schenk (1985) and McKinnon et al. (2003).

The transient crater diameter is not equal to the final crater diameter. The bowl-shaped transient crater is unstable and collapses under the influence of gravity. Scaling from transient crater to final crater size is not experimentally constrained. On Earth, craters larger than $D_{sc} \approx 2 - 4$ km have more complex morphologies, including central uplifts and peak rings. These morphologies are attributed to uplift of the crater floor during wall collapse (e.g., Melosh, 1989). Several scaling laws based on detailed observation of craters and their ejecta, as well as reconstructions of transient crater geometry, have been used to produce relationships between transient crater and final crater diameter (Croft, 1985; Holsapple, 1993; Schenk and McKinnon, 1985). Correct application of these expressions requires careful attention to the definitions of pre- and post-collapse crater diameters, measured either at the level of the pre-impact surface or at the crater rim. As Eq. (1) defines the diameter at the pre-impact level, here we take care to relate that measure of the transient crater (D_{trans}) to the final crater diameter measured at the rim crest (D_{final}). The increase in crater diameter therefore results from both crater enlargement by rim collapse and the inward-dipping slope of the rim.

Grieve and Garvin (1984) describe a well-tested geometric model for the collapse of simple craters. This model, under the assumption of a 5–10% increase in the volume of the collapsing rim material to account for shear bulking, suggests that the ratio $\gamma = \frac{D_{final}}{D_{trans}}$ (the final crater diameter measured at the rim crest divided by the transient crater diameter measured at the pre-impact level) is 1.23–1.28. This brackets the $\gamma = 1.25$ assumed by Collins et al. (2005).

Several authors (e.g., Croft, 1985; Schenk and McKinnon, 1985, Holsapple, 1993) describe similar geometric models for complex crater formation. To combine with Eq. (1), these equations should take the general form:

$$D_{final} = AD_{sc}^{-\eta} D_{trans}^{1+\eta} \quad (2)$$

where D_{sc} is the final rim diameter at the simple-to-complex transition and A and η are constants. However, to compare these models it is crucial that a consistent definition of D_{trans} is used. Although these equations all seek to relate final crater diameter to transient crater diameter they are most informatively compared when expressed in the form:

$$\frac{D_{final}}{D_{eqs}} = \left(\frac{D_{eqs}}{D_{sc}} \right)^\eta \quad (3)$$

where D_{sc} is the final rim diameter at the simple-to-complex transition, $D_{eqs} = \gamma D_{trans}$ is the final rim diameter of the “equivalent simple crater” and η is the same constant as in Eq. (2). This form is convenient because the enlargement factor is 1 at the simple-to-complex transition and increases monotonically as crater size increases (the equation does not apply for $D_{eqs} < D_{sc}$). When expressed in this form, the three geometric models of complex crater collapse in wide use can be described by η and $\gamma = A^{\frac{1}{1+\eta}}$, the ratio of final to transient crater diameter for simple craters (Table 2).

A comparison of the complex crater collapse models of Croft (1985), Schenk and McKinnon (1985) and Holsapple (1993) reveals

that they (apparently) make quite disparate assumptions regarding crater enlargement for craters with diameters below the simple-complex transition, ranging from $\gamma = 1$ (i.e., no collapse; Croft, 1985) to $\gamma = 1.32$ (Holsapple, 1993). The assumption of $\gamma = 1$ is not appropriate for two reasons. First, both geometric and numerical models of simple crater formation show that substantial enlargement occurs in large simple craters via debris sliding of the over-steepened transient crater rim walls. Second, a value of $\gamma = 1$ only makes sense if the transient crater diameter is measured at the rim; according to the transient crater diameter definition preferred here, γ must be 5–10% larger to account for the slope of the transient crater rim above the preimpact surface. This latter observation also applies to the value of $\gamma = 1.15$ adopted by Schenk and McKinnon (1985), because they also defined the transient crater diameter at the transient crater rim. In this case, the implied value of γ , as defined here, would be about ≈ 1.24 (Fig. 7 in Schenk and McKinnon, 1985). To adjust both of these models to use transient crater diameter at the pre-impact level (and account for simple crater collapse) we have redefined the value of A in Eq. (2) for each model assuming $\gamma = 1.25$, as suggested by the geometric model of simple crater collapse proposed by Grieve and Garvin (1984) (modified model parameters in Table 2). We note that as this modification leaves Eq. (3) unchanged, it has no consequence for how each model was derived from observations. Holsapple (1993) based his assumption of $\gamma = 1.32$ (which adopts the same transient crater diameter definition as used here) on measured shapes and rim profiles of craters produced in small-scale laboratory cratering experiments, which are often regarded as “frozen” transient craters. Although this is somewhat larger than 1.25 it has a sound basis and serves as a useful measure of uncertainty in simple crater enlargement. We therefore retain it for our analysis rather than modifying it to assume a consistent value of γ across all (modified) models.

Fig. 5 compares the five complex crater collapse models given by Eq. (2) and parameters in Table 2. Both transient and final crater diameters are normalized to the simple-complex transition diameter D_{sc} . There is good agreement between the three modified models (solid lines) if the lower bound for complex crater enlargement of Croft (1985) is used. Adopting the upper bound of Croft (1985) would overestimate the final crater diameter by as much as 60% if that model was applied to the largest lunar basins. Also evident is the potential for a systematic discrepancy between models of $\sim 30\%$ in final crater diameter if inconsistent definitions of the transient crater diameter are used.

Another way to estimate final crater diameters is using detailed numerical models called hydrocodes or shock physics codes to directly model crater excavation and collapse. The iSALE shock physics code has been rigorously tested against experiment including impact and shock experiments in porous materials (Collins et al., 2011; Wünnemann et al., 2006); oblique impact experiments into strong ductile materials (Davison et al., 2011); and thin plate jetting experiments (Johnson, Bowling and Melosh, 2014). The iSALE shock physics code includes detailed constitutive relations used to model the deformation of geologic materials (Collins et al., 2004). Recently Collins (2014) added a dilatancy model, which describes how deformation increases the porosity of geological materials. Using iSALE Collins (2014) modeled the formation of terrestrial craters from roughly 2–200 km in diameter by varying impactor diameter from 0.1–20 km in diameter. In addition to matching the observed morphology of craters including the transition from simple to complex craters and the transition from central-peak to peak-ring craters, these models also reproduced the observed gravity signature of terrestrial craters (Collins, 2014).

Fig. 6 shows a comparison between the crater diameter predicted by scaling laws, (Eqs. (1) and (2)), and the model crater

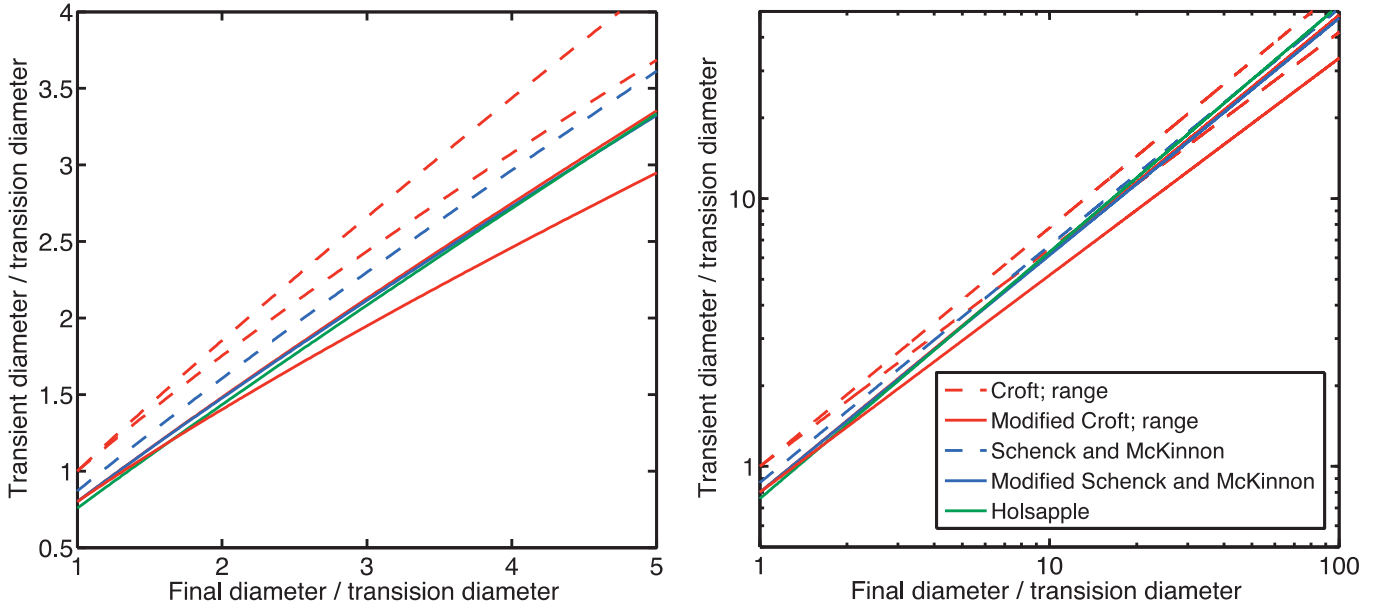


Fig. 5. Comparison of complex crater enlargement scaling laws. Transient crater diameter normalized by the simple-complex transition diameter as a function of final (rim) diameter normalized in the same way. Dashed lines show the original models of [McKinnon and Schenk \(1985\)](#) and [Croft \(1985\)](#) in which the transient crater diameter is measured at the rim. Solid lines show the modified models in which transient crater diameter is measured at the pre-impact level, for use with transient crater scaling laws. (For interpretation of the references to color in this figure legend, the reader is referred to the web version of this article.)

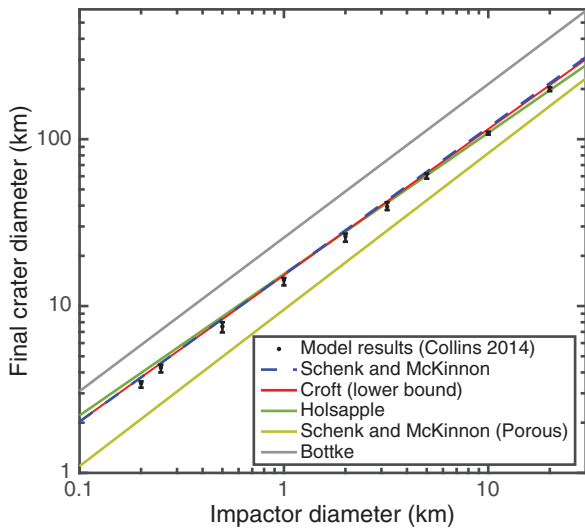


Fig. 6. Comparison of numerical impact models and crater scaling laws. The solid curves were calculated using [Eqs. \(1\) and \(2\)](#), with parameters in [Table 1](#), using the same impact conditions as those of the numerical impact models of [Collins \(2014\)](#), $v_{imp} = 15 \text{ km/s}$, $p_{imp} = p_{targ}$, $\theta = 90^\circ$, $g = 9.18 \text{ m/s}^2$, and $D_{SC} = 4 \text{ km}$. The points with error bars are the final crater diameters, for craters larger than D_{SC} , from [Collins \(2014\)](#). The main text describes how rim location and error bars are determined. The red curve shows the results obtained using the equations from the LPL calculator (equations described in text) and assuming, as [Bottke et al. \(2012, 2015\)](#) do, that an impactor of a given size produces a crater of the same size on both the Earth and the Moon. That is, $v_{imp} = 15 \text{ km/s}$, $p_{imp} = p_{targ}$, $\theta = 90^\circ$, $g = 1.67 \text{ m/s}^2$, $D_{SC} = 18 \text{ km}$. (For interpretation of the references to color in this figure legend, the reader is referred to the web version of this article.)

diameters from [Collins \(2014\)](#). The scaling law for transient crater size ([Eq. \(1\)](#)) is derived from impact experiments and the scaling laws for final crater diameter ([Eq. \(2\)](#)) are derived from observation of craters and their ejecta, as well as reconstructions of transient crater geometry. Thus numerical models of crater formation and collapse act as an independent test of these scaling laws. We determine the rim location from the models by mea-

suring the point of highest topography, measured with respect to the pre-impact surface. As rim topography tends to be smooth in the numerical simulations, introducing a small uncertainty in the exact rim location, the error bars in [Fig. 6](#) represent the innermost and outermost location where the crater reaches 90% of this highest topography. Clearly, the simple scaling laws and detailed models of crater formation are in excellent agreement.

Given the close correspondence between the numerical impact models and the (modified) complex crater collapse scaling laws, and the consistency between scaling laws, particularly those of [Croft \(1985; lower bound\)](#) and [Schenk and McKinnon \(1985\)](#), we propose that the latter model be used to derive an equation for general use that relates impactor and target properties directly to the final crater rim diameter by combining [Eqs. \(1\) and \(2\)](#):

$$D_{fin} = 1.52 \left(\frac{\rho_{imp}}{\rho_{targ}} \right)^{0.38} D_{imp}^{0.88} v_{imp}^{0.5} g^{-0.25} D_{SC}^{-0.13} \sin^{0.38}(\theta) \quad (4)$$

All of the quantities in [Eq. \(4\)](#) are in MKS units. Note that the value for the simple to complex transition D_{SC} is target body specific and that [Eq. \(4\)](#) is only valid for final craters larger than D_{SC} . We note that the $\sim 10\%$ difference between various scaling laws and numerical models ([Fig. 6](#)) can be used as a rough estimate of the error associated with [Eq. \(4\)](#).

[Fig. 6](#) shows that craters formed in non-porous targets are larger than those that form in porous targets. Producing a good match between observed sizes of lunar craters and the current day population of impactors, based on observations of NEOs and the main asteroid belt, requires a transition from porous scaling to non-porous scaling at a crater size around 0.5–10 km in diameter ([Ivanov and Hartmann, 2007](#)). Although, this does not affect our estimates of the impactor sizes needed to create large craters, for completeness, we create an equation for final crater diameter that is appropriate for impacts into porous targets. This equation uses the modified [Schenk and McKinnon \(1985\)](#) for transient to final crater scaling.

$$D_{fin} = 1.66 \left(\frac{\rho_{imp}}{\rho_{targ}} \right)^{0.38} D_{imp}^{0.94} v_{imp}^{0.38} g^{-0.19} D_{SC}^{-0.13} \sin^{0.38}(\theta) \quad (5)$$

For a typical E-belt impact with $v_{imp} = 22$ km/s, $p_{imp} \approx p_{target}$, $D_{sc} = 4$ km, and the most probable impact angle $\theta = 45^\circ$, a 13.2-km diameter impactor is required to make a Chicxulub-sized crater, $D_{final} = 160$ km, on Earth. This impactor diameter is more than a factor of two larger than that assumed to produce Chicxulub-sized craters in tests of the E-belt model (Bottke et al., 2012, 2015). E-belt impactors were initially assumed to have a SFD similar to the current main belt (Bottke et al., 2012; Minton et al., 2015b). Using the SFD of the main belt (Fig. 1), we compare the number of 6 km diameter bodies to the number of 13.2-km diameter bodies. We find that the E-belt forms 71 craters larger than 160 km in diameter on Earth over 4.1 Gyr where Bottke et al. (2012) report that 523 should form. Thus, the E-belt model overstates its consequences by a factor of more than 7.4. If instead we assume E-belt impactors had a SFD similar to Near Earth Objects (NEOs), the same comparison indicates this factor is 9.7.

For the same impact conditions above, we find a 27-km diameter impactor is required to form a 300-km diameter impact basin on Earth. Using the SFD of the main belt, we compare the number of 6-km diameter bodies to the number of 27-km diameter bodies. We find that the E-belt creates 22 basins larger than 300 km in diameter on Earth over 4.1 Gyr where Bottke et al. (2012) reports that 154 such basins should form.

Using Eq. (4) with lunar gravity $g = 1.62$ m/s², $D_{sc} = 15$ km appropriate for the Moon (Croft, 1985), $v_{imp} = 22$ km/s, $p_{imp} \approx p_{target}$, and the most probable impact angle $\theta = 45^\circ$, we find 9.7-km and 19.7-km diameter impactors are required to create 160-km and 300-km craters on the Moon, respectively. Using the main-belt SFD we compare the number of 6-km diameter bodies to the number of 9.7-km and 19.7-km diameter bodies. We find that the nominal E-belt model only creates 2 lunar craters larger than 300 km and 8.7 craters larger than 160 km in diameter in 4.1 Gyr compared to the 9.1 and 31 reported by Bottke et al. (2012), respectively.

Bottke et al. (2012, 2015) use the following LPL online calculator to estimate final crater diameter produced by a given impact (<http://www.lpl.arizona.edu/tekton/crater.html>). The source code reveals that the calculator uses Eq. (1) to calculate the transient crater diameter but the final crater diameter is calculated using $D_{final} = D_{eqs}^{1.18} / D_{sc}^{0.18}$ (Croft, 1985), where the equivalent simple crater diameter is assumed to be $D_{eqs} = 1.56 D_{trans}$ (i.e., $\gamma = 1.56$). Hence, this approach overestimates both the enlargement factor owing to simple crater collapse (γ) and the additional enlargement owing to complex crater collapse (through the exponent η). Another minor effect that contributes to the overestimate of crater sizes in Bottke et al. (2012, 2015) is the assumption that an impactor of a given size makes a crater of the same size on both the Earth and the Moon. More precisely, Bottke et al. (2012, 2015) use $g = 1.67$ m/s² and $D_{sc} = 18$ km for both the Earth and Moon.

Johnson and Bowling (2014) estimated the expected terrestrial cratering record based on different terrestrial bombardment histories. They reported that the impactors from the E-belt alone could create six craters larger than 85 km in diameter that may have survived until today (Johnson and Bowling, 2014). Unfortunately, Johnson and Bowling (2014) assumed that the number of Chicxulub-sized craters the E-belt can form reported by Bottke et al. (2012) was correct. Thus, they overestimate the contribution of the E-belt to the terrestrial cratering record by a factor of 7.5–10. Considering this, we conclude that the nominal E-belt would at most create a single crater larger than 85 km in diameter that survives to the current day on Earth. At least 6 craters of this size have been recognized on Earth. Because Bottke et al. (2012) did not report the impactor diameter assumed to make Chicxulub-sized craters, any paper using their flux estimates likely overestimates the E-belt flux by a factor of ~ 7.5 –10.

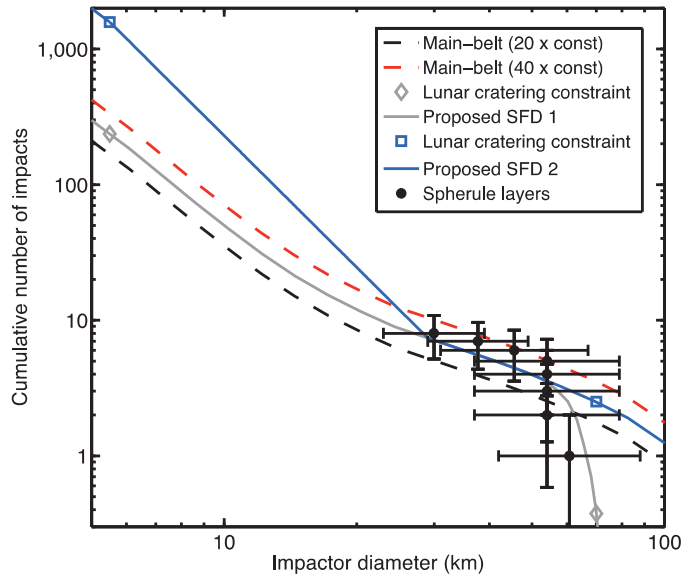


Fig. 7. Log-log plot of the cumulative number of impacts larger than a given size plotted as a function of impactor diameter. The dashed red and black curves are the same as those described in Fig. 4 and represent the main-belt SFD. The black points with error bars represent the SFD from spherule layers that formed between 3.2–3.5 Ga as described in Fig. 4. The grey diamonds show the relative number of impactors larger than 70 km in diameter and 5.5 km in diameter needed to explain the lunar cratering record. The blue squares show the same constraint but with a higher total flux. (For interpretation of the references to color in this figure legend, the reader is referred to the web version of this article.)

4. The size distribution of ancient terrestrial impactors

We have assumed that the SFD of impactors that created the spherule layers was equivalent to the main belt SFD. However, recent work shows that bombarding the Moon with a main-belt-like SFD would create an overabundance of mega-basins, craters with diameters greater than 1200 km (Minton et al., 2015b). An impactor SFD that agrees with the lunar cratering record has ~ 630 impactors larger 5.5 km in diameter for every one impactor larger than 70 km in diameter (Minton et al., 2015b). Two scenarios that adhere to this constraint are shown by the grey diamonds (scenario 1) and blue squares (scenario 2) in Fig. 7. We propose two potential SFDs that are consistent with both the lunar cratering record and the spherule layer record. These SFDs also minimize differences between the proposed SFDs and the main-belt SFD.

The grey “Proposed SFD 1” curve in Fig. 7 shows a SFD that is main-belt-like up to ~ 50 km in diameter with an abrupt steepening above 50 km. This SFD is similar to the SFDs produced by catastrophic disruption of large parent bodies (Durda et al., 2007). In a catastrophic disruption SFD the steepening occurs at diameters near the largest remaining fragment size (Durda et al., 2007). This does not match the predictions of the E-belt model (Bottke et al., 2015; 2012), but is potentially consistent with a giant impact ejecta origin for the LHB impactors and the impactors that created the Archean spherule layers (Minton et al., 2015a; Volk and Gladman, 2015). Although Fig. 3 only includes spherule layers corresponding to impactors that are ~ 20 –30 km in diameter, Fig. 4 includes spherule layers that correspond to impactors that are ~ 30 –60 km in diameter (i.e. the same size range where proposed SFD 1 becomes steep). The impactor SFD from spherule layers shown in Fig. 4 does show some steepening at the larger impactor sizes. This disagreement between the main-belt SFD and spherule layer SFD shown in Fig. 4 may be further indication that the population of ancient terrestrial impactors was something like Proposed SFD 1.

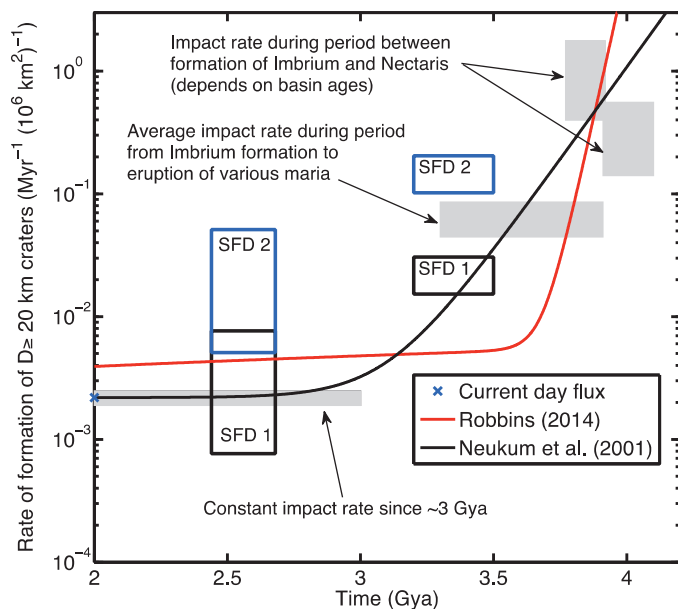


Fig. 8. Estimates of impactor flux on the Moon. The filled grey boxes are estimates made by Fassett and Minton (2013). The blue star plotted at 2 Ga is the current impactor flux according to observations of NEOs. The comparison of flux based on spherule layers to lunar cratering record assumes that 17 impactors of a given size hit the Earth for every one that hits the Moon (Bottke et al. 2012). The flux implied by the spherule layers is estimated assuming proposed SFD 1 (black boxes) and proposed SFD 2 (blue boxes). The red and black curves are best fit estimates from Neukum et al. (2001) and Robbins (2014), respectively. The curves were scaled from the rate of formation of 1 km diameter craters by normalizing to the current rate at which 20-km diameter craters form on the Moon. (For interpretation of the references to color in this figure legend, the reader is referred to the web version of this article.)

The blue “Proposed SFD 2” is main-belt like for impactors larger than 20 km in diameter and steeper than the main belt for impactors smaller than 30 km in diameter. If the E-belt had a significantly different collisional history than the main belt, this relative SFD could be consistent with the population of E-belt impactors (Bottke et al., 2015). However, the absolute E-belt flux would still be too low to explain the formation of the Archean spherule layers. “Proposed SFD 2” is similar to the SFD of asteroid families created by cratering on a large parent body (Durda et al., 2007). Because little is known about the initial SFD of giant impact ejecta, this SFD is also potentially consistent with giant impact ejecta (Jackson et al., 2014). Clearly, detailed modeling of the formation and collisional evolution of giant impact ejecta is required to determine if a giant impact ejecta origin for the LHB is consistent with constraints on the ancient impactor population.

The spherule record along with lunar cratering constraints based on the apparent lack of mega-basins (Minton et al., 2015b) allow for a range of possible impactor SFDs (Fig. 7). These SFDs, however, make completely different predictions for the number of smaller craters we expect to find on the Moon. Fassett and Minton (2013) recently compiled a variety of constraints based on the lunar cratering record (Neukum et al., 2001; Stöffler and Ryder, 2001), putting them all in terms of the rate at which craters larger than 20 km in diameter form on the Moon (Fig. 8).

To compare the spherule layer record to the lunar cratering record, we first estimate the impactor size required to make a 20-km diameter crater. Using Eq. (4) with lunar gravity $g = 1.62 \text{ m/s}^2$ and $D_{SC} = 15 \text{ km}$ appropriate for the Moon (Croft, 1985), $v_{imp} = 16 \text{ km/s}$ typical for the Moon (Yue et al., 2013), $\rho_{imp} \approx \rho_{target}$, and the most probable impact angle $\theta = 45^\circ$, we find a 1.1 km diameter impactor is required to make a 20 km diameter crater on the Moon. As shown in Section 2, the spherule layers that

formed between 2.44–2.8 Ga and 3.2–3.5 Ga are consistent with and impactor flux that is 1–10 times and 20–40 times the current day flux, respectively, for very large impactors (~ 10 – 100 km in diameter). To estimate the flux of impactors larger than 1.1 km in diameter, we then extrapolate to smaller impactor sizes using proposed SFD 1 (black boxes) and proposed SFD 2 (blue boxes) (where proposed SFD 2 is assumed to be main-belt like for impactors smaller than 5.5 km in diameter).

When using proposed SFD 1, the rate of formation of 20 km diameter craters is consistent with the lunar crater chronology of Neukum et al. (2001) (Fig. 8). Whereas, if we use proposed SFD 2 the implied flux is roughly an order of magnitude higher than the Neukum lunar cratering chronology (Fig. 8). On this basis we argue that proposed SFD 1 is more consistent with the lunar chronology than proposed SFD 2. Although proposed SFD 1 does better than proposed SFD 2, neither SFD fits the chronology of Robbins (2014). This may imply that the Neukum (2001) chronology is more representative of the terrestrial impactor flux.

5. Discussion

We note that the chronology of Robbins (2014) is in disagreement with the average rate of formation of 20-km diameter craters on the lunar maria (Fassett and Minton 2013, Fig. 8). Although, Robbins (2014) was careful to remove clusters of secondary craters, distant secondary craters may be spatially homogeneous (McEwen and Bierhaus, 2006). The only way to ensure secondary craters are omitted is to count only craters larger than $\sim 1 \text{ km}$ in diameter (McEwen and Bierhaus, 2006), but Robbins (2014) focuses on craters 1 km in diameter and smaller. Consequently, we prefer the grey boxes in Fig. 8 as constraints, as these flux estimates are based on the number of 20-km diameter craters (Fassett and Minton 2013). Clearly there are some significant uncertainties associated with interpretations of the lunar crater record.

The exceptional agreement between the current rate of formation of lunar craters larger than 20 km in diameter implied by observations of NEO’s and estimates based on lunar craters provides an independent validation of the crater scaling laws discussed in Section 3 (Fig. 8). Recent careful work interpreting the terrestrial cratering record by Hughes (2000) suggest craters larger than 20 km in diameter were created at a rate of $(3.46 \pm 0.30) \times 10^{-15} \text{ km}^{-2} \text{ yr}^{-1}$ over the past $125 \pm 20 \text{ Myr}$. This is in excellent agreement with crater scaling laws and estimates of the current day impactor flux based on observations of NEO’s. Within the reported error, the commonly used $(5.6 \pm 2.8) \times 10^{-15} \text{ km}^{-2} \text{ yr}^{-1}$ (Grieve, 1998) for the formation rate of craters larger than 20 km in diameter is consistent with estimate of Hughes (2000).

Another potential source of error comes from uncertainties in the estimates of the sizes of impactors that created the Archean spherule layers. Estimates based on layer thickness and extraterrestrial material content generally agree that the centimeters to 10’s of centimeters thick Archean spherule layers were created by impactors that were ~ 10 – 90 km in diameter (Johnson and Melosh, 2012b; Kyte et al., 2003; Lowe et al., 2003, 2014; Lowe and Byerly, 2015). However, estimates based on extraterrestrial material content may be affected by the heterogeneous distribution of Ni-rich chromium spinel which accounts for the bulk of the enrichment in platinum group elements. Additionally, many layers show signs of dilution, redeposition by surface processes, and tectonic deformation potentially affecting the thickness estimates reported in Table 1 (Lowe et al., 2003). It is also possible that some of the layers are not global vapor plume layers but are more proximal ejecta like deposits from the Sudbury or Vredefort impacts (Cannon et al., 2010; Huber et al., 2014a, 2014b). This has already been suggested for the Carawine, Jeerinah, and Dales Gorge spherule layers based on the characteristics of their spherules and related melt particles

(Simonson et al., 2000; Jones-Zimmerlin et al., 2006; Sweeney and Simonson, 2008). One test of the estimates of impactor size comes from the comparison to the lunar cratering record. For example, if the impactor flux implied by the Archean spherule layers was well above that implied by the lunar cratering record this may imply impactor sizes are consistently over estimated. Fig. 8 shows that for a reasonable impactor size frequency distribution, it is possible to reconcile the impactor flux implied by spherule layers with flux estimates based on the lunar cratering record.

When an impactor component is recognized in a spherule layer, its composition can act as a further constraint on LHB models. The Chromium isotopes in S2, S3, and S4 (from 3.2–3.5 Ga) all imply they were formed by carbonaceous chondrite impactors (Kyte et al., 2003). This is in contrast to the younger layers that formed between 2.44–2.68 Ga, which show a variety of compositions consistent with E-chondrites, martian meteorites, or ordinary chondrites (Simonson et al., 2009). The compositions of the older layers, which imply an impactor flux ~ 20 –40 the current impactor flux, may appear inconsistent with a giant impact origin for the LHB (Minton et al., 2015a; Volk and Gladman, 2015). However, if ejecta from a giant impact on Mars created the spherule layers, the common composition of S2, S3, and S4 could be explained by one of the bodies involved in the giant impact being a large carbonaceous chondrite, potentially a body similar to Ceres.

It is intriguing that the martian moons, Phobos and Deimos, appear to be a combination of martian and carbonaceous chondrite material (Citron et al., 2015). Moreover, Citron et al. (2015) suggest that Phobos and Deimos were the result of the putative Borealis-forming giant impact (Andrews-Hanna et al., 2008). The return of samples from Mars, Phobos, and Deimos along with detailed isotopic analysis could conceivably detect the signature of the putative giant impactor. Regardless of the source of the ancient impactors, the terrestrial spherule layers, when coupled with the lunar cratering record, clearly offer valuable clues about the population of ancient terrestrial impactors.

Acknowledgments

We thank Christian Koeberl and an anonymous reviewer for their helpful reviews. We also thank H. Jay Melosh for fruitful discussion and comments on an earlier version of this manuscript.

References

- Andrews-Hanna, J.C., Zuber, M.T., Banerdt, W.B., 2008. The Borealis basin and the origin of the martian crustal dichotomy. *Nature* 453, 1212–1215. doi:10.1038/nature07011.
- Bailer-Jones, C.A.L., 2011. Bayesian time series analysis of terrestrial impact cratering. *Month. Not. R. Astr. Soc.* 416, 1163–1180. doi:10.1111/j.1365-2966.2011.19112.x.
- Bottke, W.F., Marchi, S., Vokrouhlický, D., et al., 2015. New insights into the martian late heavy bombardment. In: *Proceedings of the 46th Lunar and Planetary Science Conference*, p. #1484.
- Bottke, W.F., Vokrouhlický, D., Minton, D., et al., 2012. An Archaean heavy bombardment from a destabilized extension of the asteroid belt. *Nature* 485, 78–81. doi:10.1038/nature10967.
- Cannon, W.F., Schulz, K.J., Horton Jr., J.W., et al., 2010. The Sudbury impact layer in the Paleoproterozoic iron ranges of northern Michigan, USA. *Geol. Soc. Am. Bull.* 122, 50–75. doi:10.1130/B26517.1.
- Citron, R.I., Genda, H., Ida, S., 2015. Formation of Phobos and Deimos via a giant impact. *Icarus* 252, 334–338. doi:10.1016/j.icarus.2015.02.011.
- Collins, G.S., 2014. Numerical simulations of impact crater formation with dilatancy. *J. Geophys. Res. Planets* 119. doi:10.1002/2014JE004708.
- Collins, G.S., Melosh, H.J., Ivanov, B.A., 2004. Modeling damage and deformation in impact simulations. *Meteor. Planet. Sci.* 39, 217–231. doi:10.1111/j.1945-5100.2004.tb00337.x.
- Collins, G.S., Melosh, H.J., Marcus, R.A., 2005. Earth impact effects program: A Web-based computer program for calculating the regional environmental consequences of a meteoroid impact on Earth. *Meteor. Planet. Sci.* 40, 817–840. doi:10.1111/j.1945-5100.2005.tb00157.x.
- Collins, G.S., Melosh, H.J., Wünnemann, K., 2011. Improvements to the ϵ - α porous compaction model for simulating impacts into high-porosity Solar System objects. *Int. J. Impact Eng.* 38, 434–439. doi:10.1016/j.ijimpeng.2010.10.013.
- Croft, S.K., 1985. The scaling of complex craters. *J. Geophys. Res.* 90, 828–842. doi:10.1029/JB090iS02p0C828.
- Davison, T.M., Collins, G.S., Elbeshhausen, D., et al., 2011. Numerical modeling of oblique hypervelocity impacts on strong ductile targets. *Meteor. Planet. Sci.* 46, 1510–1524. doi:10.1111/j.1945-5100.2011.01246.x.
- Durda, D.D., Bottke, W.F., Nesvorný, D., et al., 2007. Size–frequency distributions of fragments from SPH/N-body simulations of asteroid impacts: Comparison with observed asteroid families. *Icarus* 186, 498–516. doi:10.1016/j.icarus.2006.09.013.
- Fassett, C.I., Minton, D.A., 2013. Impact bombardment of the terrestrial planets and the early history of the Solar System. *Nature Geosci* 6, 520–524. doi:10.1038/ngeo1841.
- Glass, B.P., Simonson, B.M., 2012. Distal impact ejecta layers: Spherules and more. *Elements* 8, 43–48. doi:10.2113/gselements.8.1.43.
- Gomes, R., Levison, H.F., Tsiganis, K., et al., 2005. Origin of the cataclysmic Late Heavy Bombardment period of the terrestrial planets. *Nature* 435, 466–469. doi:10.1038/nature03676.
- Grieve, R.A.F., 1998. Extraterrestrial impacts on Earth: The evidence and the consequences. *Geol. Soc., Lond., Sp. Pub* 140, 105–131. doi:10.1144/GSL.SP.1998.140.01.10.
- Grieve, R.A.F., Garvin, J.B., 1984. A geometric model for excavation and modification at terrestrial simple impact craters. *J. Geophys. Res.* 89, 11561–11572. doi:10.1029/JB089iB13p11561.
- Harris, A.W., D'Abramo, G., 2015. The population of near-Earth asteroids. *Icarus* 257, 302–312. doi:10.1016/j.icarus.2015.05.004.
- Holsapple, K., 1993. The scaling of impact processes in planetary sciences. *Ann. Rev. Earth Planet. Sci.* 21, 333–373. doi:10.1146/annurev.earth.21.1.333.
- Holsapple, K.A., Schmidt, R.M., 1982. On the scaling of crater dimensions. II - Impact processes. *J. Geophys. Res.* 87, 1849–1870. doi:10.1029/JB087iB03p01849.
- Huber, M., McDonald, I., Koeberl, C., 2014. Petrography and geochemistry of ejecta from the Sudbury impact event. *Meteor. Planet. Sci.* 49, 1749–1768. doi:10.1111/maps.12352.
- Huber, M.S., Crne, A.E., McDonald, I., et al., 2014. Impact spherules from Karelia, Russia: Possible ejecta from the 2.02 Ga Vredefort impact event. *Geology* 42, 375–378. doi:10.1130/G35231.1.
- Hughes, D.W., 2000. A new approach to the calculation of the cratering rate of the Earth over the last 125 ± 20 Myr. *Mon. Not. R. Astr. Soc.* 317, 429–437. doi:10.1046/j.1365-8711.2000.03568.x.
- Ivanov, B.A., Hartmann, W.K., 2007. Planets and Moons. In: Schubert, G. (Ed.), *Treatise on Geophysics*, 10. Elsevier, pp. 202–242. doi:10.1016/B978-044452748-6.00158-9.
- Jackson, A.P., Wyatt, M.C., Bonsor, A., et al., 2014. Debris from giant impacts between planetary embryos at large orbital radii. *Mon. Not. R. Astr. Soc.* 440, 3757–3777. doi:10.1093/mnras/stu476.
- Johnson, B.C., Bowling, T.J., 2014. Where have all the craters gone? Earth's bombardment history and the expected terrestrial cratering record. *Geology* 42, 587–590. doi:10.1130/G35754.1.
- Johnson, B.C., Bowling, T.J., Melosh, H.J., 2014. Jetting during vertical impacts of spherical projectiles. *Icarus* 238, 13–22. doi:10.1016/j.icarus.2014.05.003.
- Johnson, B.C., Melosh, H.J., 2012. Formation of spherules in impact produced vapor plumes. *Icarus* 217, 416–430. doi:10.1016/j.icarus.2011.11.020.
- Johnson, B.C., Melosh, H.J., 2012. Impact spherules as a record of an ancient heavy bombardment of Earth. *Nature* 485, 75–77. doi:10.1038/nature10982.
- Johnson, B.C., Melosh, H.J., 2014. Formation of melt droplets, melt fragments, and accretionary impact lapilli during a hypervelocity impact. *Icarus* 228, 347–363. doi:10.1016/j.icarus.2013.10.022.
- Jones-Zimmerlin, S., Simonson, B.M., et al., 2006. Using impact spherule layers to correlate sedimentary successions: a case study of the Neoproterozoic Jeerinah layer (Western Australia). *S. Afr. J. Geol.* 109, 245–261. doi:10.2113/gssajg.109.1-2.245.
- Koeberl, C., Schulz, T., Reimold, W.U., 2015. Remnants of early archaic impact deposits on earth: search for a meteoritic component in the BARB5 and CT3 drill cores (Barberton Greenstone Belt, South Africa). *Proc. Eng.* 103, 310–317. doi:10.1016/j.proeng.2015.04.052.
- Koeberl, C., Schulz, T., Ozdemir, S., et al., 2015. Remnants of early archaic impact events on Earth: New studies on spherule layers from the Barberton Mountain Land, South Africa. *Early Sol. Syst. Impact Bombard.* III 3017.
- Kyte, F.T., Shukolyukov, A., Lugmair, G.W., et al., 2003. Early Archean spherule beds: Chromium isotopes confirm origin through multiple impacts of projectiles of carbonaceous chondrite type. *Geology* 283 (31). doi:10.1130/0091-7613(2003)031(0283:easbcj)2.0.co;2.
- Le Feuvre, M., Wieczorek, M.A., 2011. Nonuniform cratering of the Moon and a revised crater chronology of the inner Solar System. *Icarus* 214, 1–20. doi:10.1016/j.icarus.2011.03.010.
- Lowe, D.R., Byerly, G.R., 2015. Geologic record of partial ocean evaporation triggered by giant asteroid impacts. *Geology* 3. doi:10.1130/G36665.1, pp. 29–23.
- Lowe, D.R., Byerly, G.R., Kyte, F.T., et al., 2003. Spherule beds 3.47–3.24 billion years old in Barberton Greenstone Belt, South Africa: a record of large meteorite impacts and their influence on early crustal and biological evolution. *Astrobiology* 3, 7–48. doi:10.1089/153110703321632408.
- Lowe, D.R., Byerly, G.R., Kyte, F.T., 2014. Recently discovered 3.42–3.23 Ga impact layers, Barberton Belt, South Africa: 3.8 Ga detrital zircons, Archean impact history, and tectonic implications. *Geology* 42, 747–750. doi:10.1130/G35743.1.
- McEwen, A.S., Bierhaus, E.B., 2006. The importance of secondary cratering to age constraints on planetary surfaces. *Ann. Rev. Earth Planet. Sci.* 34, 535–567. doi:10.1146/annurev.earth.34.031405.125018.

- McKinnon, W.B., Schenk, P.M., 1985. Ejecta blanket scaling on the Moon and Inferences for projectile populations. *Lunar Planet. Sci. Conf. XVI* 544–545.
- McKinnon, W.B., Schenk, P.M., Moore, J.M., 2003. Goldilocks and the three complex crater scaling laws. In: *Proceedings of the Workshop on Impact Cratering*, p. 8047.
- Melosh, H.J., 1989. *Impact Cratering: A Geologic Process*. Oxford University Press.
- Minton, D.A., Jackson, A.P., Asphaug, E., Fassett, C.I., Richardson, J.E., 2015a. Debris From Borealis basin formation as the primary impactor population of Late Heavy Bombardment. *Early Solar System Impact Bombardment III* 3033.
- Minton, D.A., Malhotra, R., 2010. Dynamical erosion of the asteroid belt and implications for large impacts in the inner Solar System. *Icarus* 207, 744–757. doi:10.1016/j.icarus.2009.12.008.
- Minton, D.A., Richardson, J.E., Fassett, C.I., 2015b. Re-examining the main asteroid belt as the primary source of ancient lunar craters. *Icarus* 247, 172–190. doi:10.1016/j.icarus.2014.10.018.
- Mohr-Westheide, T., Reimold, W.U., Fritz, J., et al., 2015. Discovery of extraterrestrial component carrier phases in Archean spherule layers: Implications for estimation of Archean bolide sizes. *Geology* 43, 299–302. doi:10.1130/G36548.1.
- Morbidelli, A., Marchi, S., Bottke, W.F., et al., 2012. A sawtooth-like timeline for the first billion years of lunar bombardment. *Earth Planet. Sci. Lett* 144–151. doi:10.1016/j.epsl.2012.07.037.
- Nesvorný, D., Vokrouhlický, D., Bottke, W.F., et al., 2007. Express delivery of fossil meteorites from the inner asteroid belt to Sweden. *Icarus* 188, 400–413. doi:10.1016/j.icarus.2006.11.021.
- Neukum, G., Ivanov, B.A., Hartmann, W.K., 2001. Cratering records in the inner solar system in relation to the lunar reference system. *Space Sci. Rev.* 96, 55–86. doi:10.1023/A:1011989004263.
- Robbins, S.J., 2014. New crater calibrations for the lunar crater-age chronology. *Earth Planet. Sci. Lett.* 403, 188–198. doi:10.1016/j.epsl.2014.06.038.
- Schenk, P.M., McKinnon, W.B., 1985. Dark halo craters and the thickness of grooved terrain on Ganymede. *J. Geophys. Res.* 90, 775. doi:10.1029/JB090iS02p0C775.
- Schmidt, R.M., Housen, K.R., 1987. Some recent advances in the scaling of impact and explosion cratering. *Int. J. Impact Eng.* 5, 543–560. doi:10.1016/0734-743x(87)90069-8.
- Simonson, B.M., Glass, B.P., 2004. Spherule Layers—Records of ancient impacts. *Ann. Rev. Earth Planet. Sci.* 32, 329–361. doi:10.1146/annurev.earth.32.101802.120458.
- Simonson, B.M., Hornstein, M., Hassler, S.W., 2000. Particles in late Archean Carawine Dolomite (Western Australia) resemble Muong Nong-type tektites. In: Gilmour, I., Koeberl, C. (Eds.), *Impacts and the Early Earth*. Springer-Verlag, pp. 181–213. doi:10.1007/BFb0027760.
- Simonson, B.M., McDonald, I., Shukolyukov, A., et al., 2009. Geochemistry of 2.63–2.49 Ga impact spherule layers and implications for stratigraphic correlations and impact processes. *Precambrian Res* 175, 51–76. doi:10.1016/j.precamres.2009.08.004.
- Smit, J., 1999. The global stratigraphy of the Cretaceous-Tertiary boundary impact ejecta. *Annu. Rev. Earth Planet. Sci.* 27, 75–113. doi:10.1146/annurev.earth.27.1.75.
- Stöffler, D., Ryder, G., 2001. Stratigraphy and isotope ages of lunar geologic units: Chronological standard for the inner solar system. *Space Sci. Rev.* 96, 9–54. doi:10.1007/978-94-017-1035-0_2.
- Stuart, J.S., Binzel, R.P., 2004. Bias-corrected population, size distribution, and impact hazard for the near-Earth objects. *Icarus* 170, 295–311. doi:10.1016/j.icarus.2004.03.018.
- Sweeney, D., Simonson, B.M., 2008. Textural constraints on the formation of impact spherules: A case study from the Dales Gorge BIF, Paleoproterozoic Hamersley Group of Western Australia. *Meteor. Planet. Sci.* 43, 2073–2087. doi:10.1111/j.1945-5100.2008.tb00662.x.
- Volk, K., Gladman, B., 2015. Consolidating and Crushing exoplanets: Did it happen here? *ApJ* 806, L26. doi:10.1088/2041-8205/806/2/L26.
- Wünnemann, K., Collins, G.S., Melosh, H.J., 2006. A strain-based porosity model for use in hydrocode simulations of impacts and implications for transient crater growth in porous targets. *Icarus* 180, 514–527. doi:10.1016/j.icarus.2005.10.013.
- Yue, Z., Johnson, B.C., Minton, D.A., et al., 2013. Projectile remnants in central peaks of lunar impact craters. *Nature Geosci* 6, 435–437. doi:10.1038/ngeo1828.